SCIENTIFIC REPORTS

OPEN

SUBJECT AREAS:
MOLECULAR BIOLOGY
GENETIC VECTORS

Received
21 January 2014

Accepted
14 May 2014

Published
29 May 2014

Correspondence and requests for materials should be addressed to M.A.F.V.G. (m.goncalves@lumc.nl)

* These authors contributed equally to this work.

Adenoviral vector delivery of RNA-guided CRISPR/Cas9 nuclease complexes induces targeted mutagenesis in a diverse array of human cells

Ignazio Maggio*, Maarten Holkers*, Jin Liu, Josephine M. Janssen, Xiaoyu Chen & Manuel A. F. V. Gonçalves

Department of Molecular Cell Biology, Leiden University Medical Center, Einthovenweg 20, 2333 ZC Leiden, The Netherlands.

CRISPR/Cas9-derived RNA-guided nucleases (RGNs) are DNA targeting systems, which are rapidly being harnessed for gene regulation and gene editing purposes in model organisms and cell lines. As *bona fide* gene delivery vehicles, viral vectors may be particularly fit to broaden the applicability of RGNs to other cell types including dividing and quiescent primary cells. Here, the suitability of adenoviral vectors (AdVs) for delivering RGN components into various cell types is investigated. We demonstrate that AdVs, namely second-generation fiber-modified AdVs encoding Cas9 or single guide RNA (gRNA) molecules addressing the Cas9 nuclease to the *AAVS1* "safe harbor" locus or to a recombinant model allele can be produced to high-titers (up to 20 × 10^{10} transducing units/ml). Importantly, AdV-mediated transduction of gRNA:Cas9 ribonucleoprotein complexes into transformed and non-transformed cells yields rates of targeted mutagenesis similar to or approaching those achieved by isogenic AdVs encoding TALENs targeting the same *AAVS1* chromosomal region. RGN-induced gene disruption frequencies in the various cell types ranged from 18% to 65%. We conclude that AdVs constitute a valuable platform for introducing RGNs into human somatic cells regardless of their transformation status. This approach should aid investigating the potential and limitations of RGNs in numerous experimental settings.

Genome engineering strategies based on designer nucleases can be harnessed to edit and to interrogate the function of genomic sequences in cells of higher eukaryotes. In common, these approaches entail the activation of cellular DNA repair pathways in target cells upon the induction of double-stranded DNA breaks (DSBs) at predefined chromosomal positions[1,2]. The engagement of non-homologous end-joining (NHEJ) and homologous recombination (HR) machineries at these artificially created DSBs can result in targeted gene knockout and addition, respectively. The potential of genome engineering is considerable for fundamental and applied research. For instance, in the form of new molecular medicine modalities such "genome surgery" approaches might constitute a watershed departure from canonical gene therapy in which chromosomal insertion of the therapeutic DNA is unpredictable[3].

Programmable nuclease technologies are developing at a rapid pace[1,2]. These include zinc-finger nucleases (ZFNs), engineered homing endonucleases, transcription activator-like effector nucleases (TALENs) and, more recently, RNA-guided nucleases (RGNs). RGNs are RNA-dependent DNA nucleases built on components from type II clustered regularly interspaced short palindromic repeat (CRISPR)-associated (Cas) systems. These systems have been evolving in bacteria and archaea as adaptive immune mechanisms against nucleic acids of foreign agents such as plasmids and phages[4,5]. CRISPR loci contain an array of short palindromic repeats separated by protospacer DNA snippets of about 20 bp that have been acquired from such invading agents. Following expression, the short palindromic repeats in precursor CRISPR transcripts (pre-crRNA) hybridize to a portion of a trans-activating CRISPR RNA (tracrRNA). The bound tracrRNA, in concert with RNase III and Cas9, lead to the processing of the pre-crRNA into small CRISPR RNAs (crRNAs) each of which encompasses a sequence complementary to a specific protospacer. Finally, crRNAs base-paired to tracrRNAs loaded with Cas9 nucleases direct site-specific DNA cleavage following crRNA:target DNA hybridization. Of note, the fact that foreign DNA harbors a so-called protospacer adjacent motif (PAM) next to the protospacer sequence whereas

crRNAs lack this PAM motif, ensures that crRNA:tracrRNA:Cas9 complexes recognize exclusively the incoming exogenous DNA as opposed to the chromosomal CRISPR-incorporated protospacers[4,5].

The above-described fundamental insights combined with enticing work done *in vitro* and in bacteria[6,7] led the type II CRISPR/Cas9 system from *Streptococcus pyogenes* to be rapidly adapted as a gene editing toolbox for mammalian cells[8–10]. These studies comprised the transfection of cell lines with plasmids expressing from RNA polymerase II (Pol-II) and Pol-III promoters, respectively, Cas9 proteins and chimeric single guide RNAs (gRNAs). The gRNAs are engineered by fusing sequence-tailored crRNAs to tracrRNA scaffolds. Thus, gRNAs are bifunctional molecules[7] consisting of crRNA targeting and tracrRNA scaffolding moieties. Owing to the fact that RGN target site specificity is governed by RNA-DNA hybridizations, as opposed to protein-DNA interactions, makes CRISPR/Cas-based systems unique among customizable nucleases. Importantly, this RNA-dependent DNA recognition feature allows for facile nuclease retargeting and multiplexing by simply replacing the RNA component of each ribonucleoprotein complex[1,11]. However, independent studies carried out in cell lines indicate that RGNs display high levels of off-target DNA cleaving activities especially when compared to protein-based platforms such as TALENs with a tradeoff existing between activity and specificity[12–16]. The off-target cleaving profile of programmable nucleases is, clearly, a parameter to take into consideration in the context of both therapeutic and basic-research protocols.

To expand the range of experimental systems in which RGNs can be tested and optimized, it is crucial to introduce these rather large macromolecular complexes not only into established cell lines but also into non-transformed diploid cell types (i.e. Cas9: 1,368 aa; 158 kDa; *Cas9* ORF: 4.1 kb). In this regard, adenoviral vectors (AdVs) constitute interesting RGN delivery candidates especially owing to their episomal nature, large cloning capacity, high-titers and ability to transduced dividing as well as non-dividing cells[17].

In the present work, we sought to investigate the capacity of AdVs for packaging and delivering functional *gRNA* and human codon-optimized *Cas9* transcriptional units into human cells. To this end, we selected previously validated gRNA molecules whose sequences target Cas9 to the so-called *AAVS1* "safe harbor" locus located on the long arm of the human chromosome 19 (19q13.42-qter)[10] or to a recombinant model allele consisting of a chromosomally integrated *eGFP* expression unit. In parallel, to serve as a reference, we took along in these transduction experiments isogenic AdVs encoding TALENs, which have also been previously validated and target the same *AAVS1* region[18]. By deploying targeted mutagenesis assays as well as live-cell readouts based on fluorescence microscopy and flow cytometry, we demonstrate that AdVs can efficiently transfer functional RGN components into human cells regardless of their transformation status.

Results

Adenoviral vectors encoding RGN components can be produced at high-titers. We started by investigating the feasibility of producing AdVs containing *Cas9* and *gRNA* transcriptional units. For this purpose, we selected early region 1 (*E1*)- and early region 2A (*E2A*)-deleted AdVs displaying fiber motifs recognizing the ubiquitous cellular receptor CD46 (Fig. 1A). This retargeted second-generation AdV system offers several advantages when compared to its conventional *E1*-deleted AdV counterpart including higher genetic capacity, lower levels of "leaky" viral gene expression and efficient transduction of cells lacking, or with low amounts of, the coxsackievirus-adenovirus receptor CAR on their surface. Among these are human cell types often utilized in experimental and applied research settings such as hematopoietic cells, skeletal muscle progenitor cells (hereinafter referred to as myoblasts), and bone marrow-derived mesenchymal stromal cells (hMSCs)[19–22].

In the current work we selected the previously validated gRNA_AAVS1-T2 unit[10], herein named $gRNA^{S1}$, to edit endogenous chromosomal sequences via AdV delivery of CRISPR/Cas9-derived RGNs. The nucleotide sequence of this gRNA targets the Cas9 nuclease to the human *AAVS1* locus (Fig. 1B). To serve as a reference, we took along the optimized designer nuclease pair TALEN-L^{S1}/TALEN-R^{S1} whose DNA-binding motifs are specific for the same *AAVS1* region[18] (Fig. 1B). We placed the ORFs coding for the *AAVS1*-specific TALENs under the control of the same transcriptional elements regulating *Cas9* expression. To this end, AdV shuttle plasmids expressing *Cas9*, *TALEN-*L^{S1} or *TALEN-*R^{S1} from the Pol-II *PGK* promoter and short *gRNA*^{S1} molecules from the Pol-III *U6* promoter, were constructed. The preference for the *PGK* promoter was motivated by its ubiquitous expression in a diverse array of human cell types and, owing to its human origin, higher resistance to silencing phenomena than that offered by commonly-used viral transcriptional elements.

Transient transfection experiments using as readout a surrogate DSB formation assay dependent on the NHEJ DNA repair pathway, showed that co-transfecting test cells with $gRNA^{S1}$- and Cas9-encoding AdV shuttle plasmids resulted in *AAVS1* targeted mutagenesis (Fig. 2). The functionality of the AdV shuttle plasmids encoding the *AAVS1*-specific TALENs was also confirmed through similar transient transfection experiments (not shown). Next, we used these validated reagents to assemble full-length AdV molecular clones for rescuing and propagating the *E1*- and *E2A*-deleted ($AdV^{\Delta 2}$) fiber-modified (F^{50}) vectors $AdV^{\Delta 2}$P.Cas9.F^{50}, $AdV^{\Delta 2}$U6.gRNA^{S1}.F^{50}, $AdV^{\Delta 2}$P.TALEN-L^{S1}.F^{50} and $AdV^{\Delta 2}$P.TALEN-R^{S1}.F^{50}. Following the rescue, propagation and purification of AdV particles, we determined that the AdV functional titers in the resulting preparations were within the typical range expected for these research-scale production rounds (i.e. 23.7×10^{10}, 13.3×10^{10}, 2.4×10^{10} and 4.2×10^{10} TU/ml for $AdV^{\Delta 2}$P.Cas9.F^{50}, $AdV^{\Delta 2}$U6.gRNA^{S1}.F^{50}, $AdV^{\Delta 2}$P.TALEN-L^{S1}.F^{50} and $AdV^{\Delta 2}$P.TALEN-R^{S1}.F^{50}, respectively). In addition, as previously shown for AdVs harboring *TALEN* expression units[18], structural analysis of packaged AdV genomes isolated from purified particles of $AdV^{\Delta 2}$P.Cas9.F^{50} and $AdV^{\Delta 2}$U6.gRNA^{S1}.F^{50} revealed restriction patterns diagnostic for AdV backbones containing intact transgenes (Fig. 3).

AdVs deliver functional RGN complexes into human cells inducing robust site-specific mutagenesis at native and recombinant target chromosomal loci. Subsequently, we sought to test via transduction experiments followed by gene knockout assays, the functionality of the $gRNA^{S1}$- and Cas9-encoding AdVs in a panel of human cell types. These target cells comprised cervix carcinoma HeLa cells, osteosarcoma U2OS cells, hMSCs and myoblasts. In addition, we took advantage of the fine-tuned adenoviral infection mechanism to introduce into target cell nuclei a range of well-defined dosages of DNA templates encoding each RGN component. Related to this, it is noteworthy mentioning that, as of yet, bipartite CRISPR/Cas nuclease complexes have been introduced into target cells mostly by transfection-based protocols deploying fixed amounts of the two RGN components. In this regard it is relevant pointing out that in contrast to ZFNs and TALENs, in which the deployment of equimolar amounts of similarly sized monomers directly follows from their *modus operandi* (i.e assembly of catalytically active dimers at the target site), RGN activities might improve by optimizing total and relative quantities of *gRNA* and *Cas* templates. Therefore, for the experiments deploying $AdV^{\Delta 2}$P.Cas9.F^{50} and $AdV^{\Delta 2}$U6.gRNA^{S1}.F^{50} we set-up "co-transduction grids" to determine gene disruption levels resulting from different combined dosages as well as ratios of the two RGN elements. Transduction experiments in the HeLa and U2OS cell lines led to dose-dependent *AAVS1* disruption following AdV-mediated gene transfer as revealed by the detection of NHEJ-derived small insertions/deletions (indels) at the target site (Fig. 4,

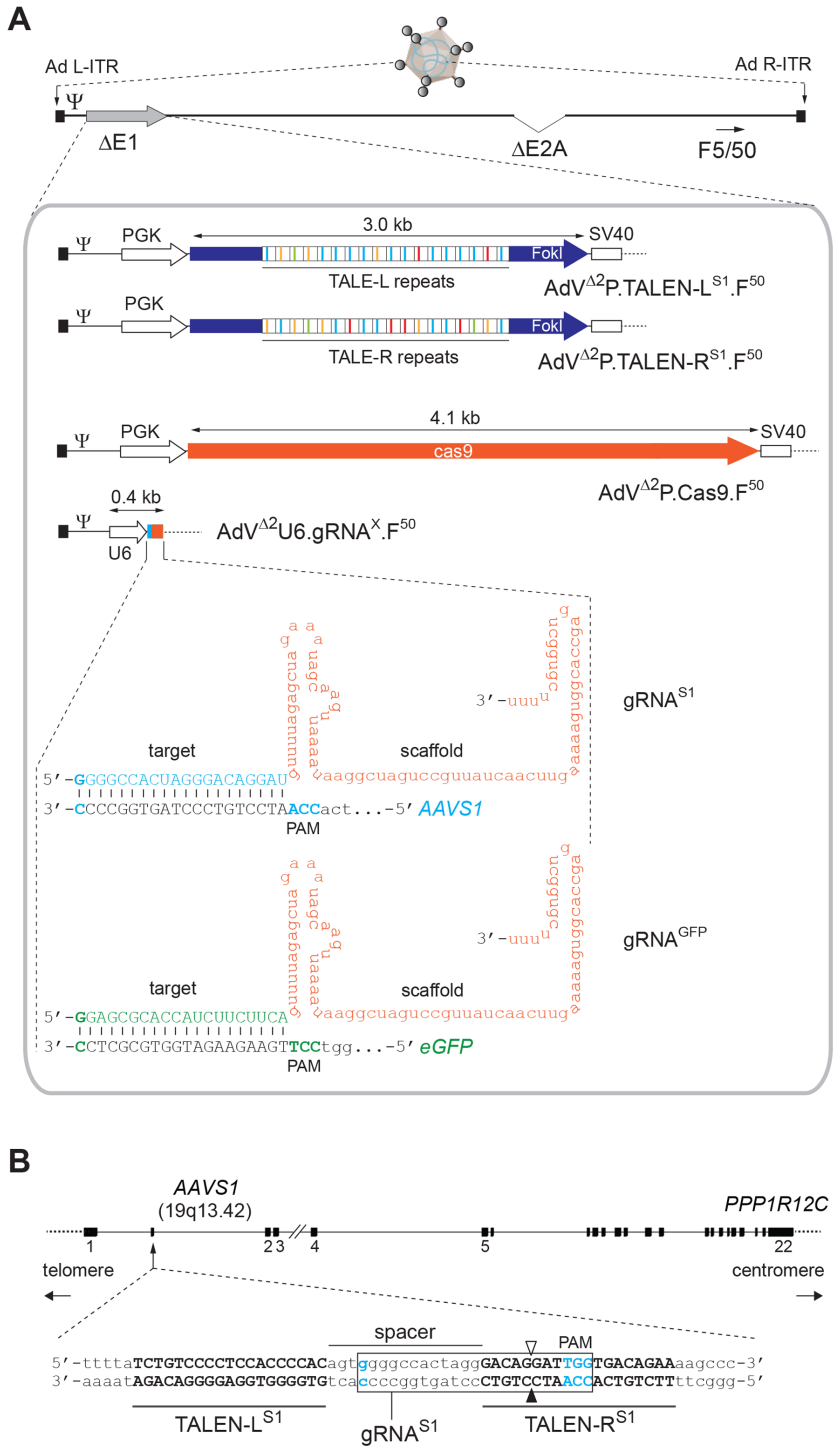

Figure 1 | Schematic representation of the genome-modifying AdVs deployed in this study and corresponding target sequences. (A) Composition of AdVs. The AdVs encode the Cas9 nuclease or TALEN proteins specific for the human "safe harbor" locus *AAVS1* within *PPP1R12C* or gRNA molecules addressing Cas9 to *AAVS1* or to *eGFP* sequences. All vectors were assembled on the basis of a second-generation (i.e. *E1*- plus *E2A*-deleted) AdV backbone ($AdV^{\Delta 2}$) coding for chimeric fibers composed of basal domains from prototypic human adenovirus serotype 5 fused to the apical shaft and knob motifs from human adenovirus serotype 50 (F5/50). The *Cas9* and *TALEN* ORFs are under the transcriptional control of the human *PGK-1* gene promoter (PGK) and the simian virus 40 (SV40) polyadenylation signal whilst the *gRNAs* are regulated by a RNA Pol-III promoter (*U6*) and terminator sequences. **Ψ**, human adenovirus serotype 5 packaging signal; Ad L-ITR and Ad R-ITR, "left" and "right" adenoviral inverted terminal repeat, respectively. The structure of the single guide RNA molecules $gRNA^{S1}$ and $gRNA^{GFP}$, composed of Cas9 targeting and scaffolding portions, are depicted base-paired to their respective *AAVS1* and *eGFP* target sequences. TALE-L and TALE-R, *AAVS1*-binding transcription activator-like effector repeats of designer nucleases TALEN-L and TALEN-R, respectively (*TALEN* portions coding for repeat variable di-residues [RVDs] recognizing A, T, C and G are color-coded); FokI, DNA portion coding for the nuclease domain of the type IIS restriction enzyme FokI; PAM, protospacer adjacent motif. (B) Target sequences. Location of the *AAVS1* target sites for the RNA- and TALE-guided nuclease complexes $gRNA^{S1}$:Cas9 and $TALEN\text{-}L^{S1}$:$TALEN\text{-}R^{S1}$, respectively, in relation to the whole *PPP1R12C* gene. The target sequences for the $TALEN\text{-}L^{S1}$ and $TALEN\text{-}R^{S1}$ proteins are in upper case, whereas that for the $gRNA^{S1}$ is boxed (i.e. $G[N]_{19}NGG$). Solid and open vertical arrowheads indicate the positions at which DNA nicking takes place catalyzed by the two nuclease domains of Cas9.

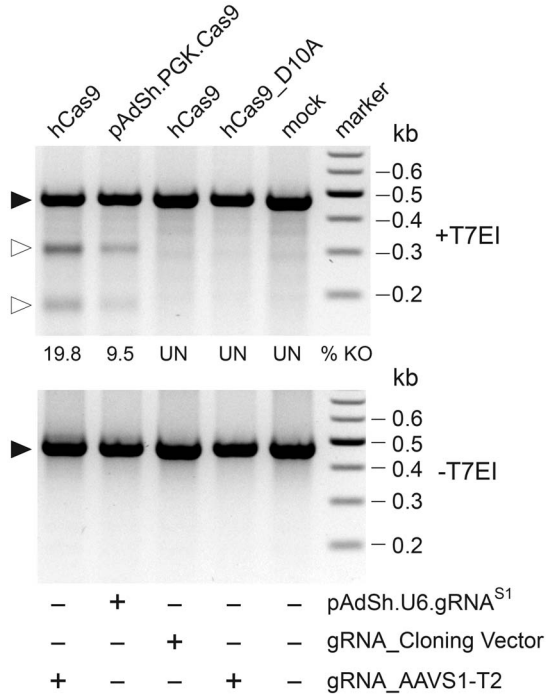

Figure 2 | Transient transfection experiments for validating AdV shuttle plasmids pAdSh.PGK.Cas9 and pAdSh.U6.gRNA^{S1}. *AAVS1*-specific PCR products amplified from *E1*-transformed PER.C6 cells co-transfected with hCas9 (9.6 kb) and gRNA_AAVS1-T2 (4 kb), pAdSh.PGK.Cas9 (11.6 kb) and pAdSh.U6.gRNA^{S1} (7.3 kb), hCas9 and "empty gRNA" construct gRNA_Cloning Vector (3.9 kb), hCas9_D10A (9.6 kb) and gRNA_AAVS1-T2 or mock-transfected. Marker, Gene Ruler DNA Ladder (Fermentas). Plasmids hCas9 and hCas9_D10A express Cas9 nucleases which induce a DSB and a nick at *AAVS1*, respectively. After amplicon denaturation and reannealing, the presence of mismatches derived from NHEJ-mediated repair of site-specific DSBs *in cellula* was probed by T7 endonuclease I (T7EI) digestions (upper panel). Negative controls were provided by amplicons not exposed to T7EI (-T7EI) as well as T7EI-treated amplicons (+T7EI) corresponding to mock-transfected cells, to cells co-transfected with hCas9 and gRNA_Cloning Vector and to cells co-transfected with hCas9_D10A and gRNA_AAVS1-T2 encoding the "nickase" mutant version of Cas9 (i.e. Cas9^{D10A}) and gRNA^{S1}, respectively. Solid and open arrowheads indicate the positions of, respectively, undigested and T7EI-digested DNA fragments whose sizes are consistent with DSB formation at the *AAVS1* target site. % KO and UN, knockout frequency and undetected, respectively.

Fig. 5A and Fig. 5B). Importantly, control transduction experiments in which only one of the two vectors was used did not result in detectable indel formation (Fig. 4). Moreover, co-transduction experiments in U2OS cells deploying side-by-side vector pairs AdV$^{\Delta2}$P.Cas9.F^{50}/AdV$^{\Delta2}$U6.gRNA^{S1}.F^{50} and AdV$^{\Delta2}$P.TALEN-L^{S1}.F^{50}/AdV$^{\Delta2}$P.TALEN-R^{S1}.F^{50} showed that, in addition to a clear AdV dose dependency, the gene knockout frequencies achieved by gRNA^{S1}:Cas9 and TALEN-L^{S1}:TALEN-R^{S1} complexes were similar (compare Fig. 5B with the lower panel in Fig. 5C).

Follow-up transduction experiments in myoblasts generally yielded results similar to those obtained in HeLa and U2OS cells. Crucially, at matched MOIs, the levels of RGN-induced targeted mutagenesis were higher in myoblasts than in the two cancer-derived cell lines (Fig. 6A and Fig. 6B). For instance, 1 : 1 mixtures of AdV$^{\Delta2}$P.Cas9.F^{50} and AdV$^{\Delta2}$U6.gRNA^{S1}.F^{50} corresponding to a combined MOI of 60 TU/cell led to gene disruption frequencies in HeLa, U2OS and myoblasts of 12%, 12% and 27%, respectively (compare Fig. 4B and Fig. 5B with Fig. 6B). Importantly, myoblasts exposed to only one of the two RGN or TALEN pair members did not contain detectable indels at *AAVS1*. Finally, it is also noteworthy pointing out that at the high-end of the MOI scale tested in myoblasts (i.e. double dose of 30 TU/cell) the AdV$^{\Delta2}$P.TALEN-L^{S1}.F^{50}/AdV$^{\Delta2}$P.TALEN-R^{S1}.F^{50} set yielded roughly a 2-fold higher gene knockout activity when compared to equivalent MOIs of the AdV$^{\Delta2}$P.Cas9.F^{50}/AdV$^{\Delta2}$U6.gRNA^{S1}.F^{50} pair (compare Fig. 6B with the lower panel in Fig. 6C). To establish the AdV transduction levels achieved in the CRISPR/Cas9-mediated targeted mutagenesis experiments corresponding to Figs. 4, 5 and 6, the various target cell types were exposed to particles of AdV$^{\Delta2}$U6.gRNA^{S1}.F^{50} and reporter vector AdV$^{\Delta2}$P.eGFP.F^{50} under the same conditions as those used in transduction experiments with AdV$^{\Delta2}$U6.gRNA^{S1}.F^{50} and AdV$^{\Delta2}$P.Cas9.F^{50}. Of note, the transgene regulatory elements in AdV$^{\Delta2}$P.eGFP.F^{50} are identical to those in AdV$^{\Delta2}$P.Cas9.F^{50}. Flow cytometric analyses clearly showed that the panel of MOIs selected for transducing each of the target cell types led to a wide range of gene delivery activities. Among these were MOIs yielding transduction levels of 100% (Supplementary Fig. 1).

In order to gather more information on target gene disruption activities attainable with the *AAVS1*-specific TALENs and RGN complexes within specific cell types and, simultaneously, probe for possible cell type-dependent effects on these activities following AdV-mediated gene transfer, we carried out parallel co-transduction experiments with both AdV sets on myoblast and hMSC cultures. In addition, to evaluate the impact of different relative concentrations of gRNA^{S1} and Cas9 molecules on gene knockout levels, we exposed these target cells to a constant total vector dose of 80 TU/cell spanning different ratios between AdV$^{\Delta2}$P.Cas9.F^{50} and AdV$^{\Delta2}$U6.gRNA^{S1}.F^{50}. The results depicted in Fig. 7A and in Fig. 7B corroborated the data on the higher TALEN pair activity in myoblasts presented in Fig. 6C and extended it to hMSCs. Indeed, gene knockout frequencies in myoblasts and hMSCs exposed to vector mixtures consisting of different ratios between AdV$^{\Delta2}$P.Cas9.F^{50} and AdV$^{\Delta2}$U6.gRNA^{S1}.F^{50} were consistently lower than those resulting from co-transductions with 1 : 1 mixtures of AdV$^{\Delta2}$P.TALEN-L^{S1}.F^{50} and AdV$^{\Delta2}$P.TALEN-R^{S1}.F^{50}. Of note, T7 endonuclease I (T7EI)-digested DNA species corresponding to genomic DNA from cells transduced with the two nuclease systems displayed different migration profiles upon electrophoresis (Fig. 7A). These molecular weight differences are consistent with the predicted target site cleaving positions for the TALEN and RGN complexes i.e. within the spacer and three nucleotides "upstream" of the PAM, respectively (Fig. 1B). AdV transduction levels corresponding to these targeted mutagenesis experiments in myoblasts and hMSCs were determined by applying AdV$^{\Delta2}$U6.gRNA^{S1}.F^{50} and AdV$^{\Delta2}$P.eGFP.F^{50} (Fig. 7C) under the same experimental conditions as those used with AdV$^{\Delta2}$U6.gRNA^{S1}.F^{50} and AdV$^{\Delta2}$P.Cas9.F^{50} (Fig. 7B). Collectively, these experiments also demonstrated that, at equivalent MOIs, AdV delivery of the *AAVS1*-specific RGNs resulted in higher gene disruption levels in myoblasts than in hMSCs regardless of the proportions of each vector type in the co-transducing AdV$^{\Delta2}$P.Cas9.F^{50}/AdV$^{\Delta2}$U6.gRNA^{S1}.F^{50} mixtures (Fig. 7D).

To further test the AdV system as a delivery platform for CRISPR/Cas9-derived RGNs, AdV$^{\Delta2}$U6.gRNA^{GFP}.F^{50} was generated. This vector has the genetic make-up of AdV$^{\Delta2}$U6.gRNA^{S1}.F^{50} except that it encodes the *eGFP*-specific gRNA^{GFP} in place of gRNA^{S1} (Fig. 1A). As with the other genome-modifying AdVs, AdV$^{\Delta2}$U6.gRNA^{GFP}.F^{50} could also be produced to high titers of functional vector particles (i.e. 10.4×10^{10} TU/ml). Next, AdV$^{\Delta2}$U6.gRNA^{GFP}.F^{50} was deployed together with AdV$^{\Delta2}$P.Cas9.F^{50} in transduction experiments in indicator H27 cells[23]. These cells contain a single-copy constitutionally active *eGFP* transcriptional unit providing, as a result, a convenient model system to evaluate target gene knockout strategies by live-cell tracing and quantification of gene-modified populations. Thus, as in experiments using AdV$^{\Delta2}$P.Cas9.F^{50} and AdV$^{\Delta2}$U6.gRNA^{S1}.F^{50}, we set-up a "co-transduction grid" to determine targeted mutagenesis

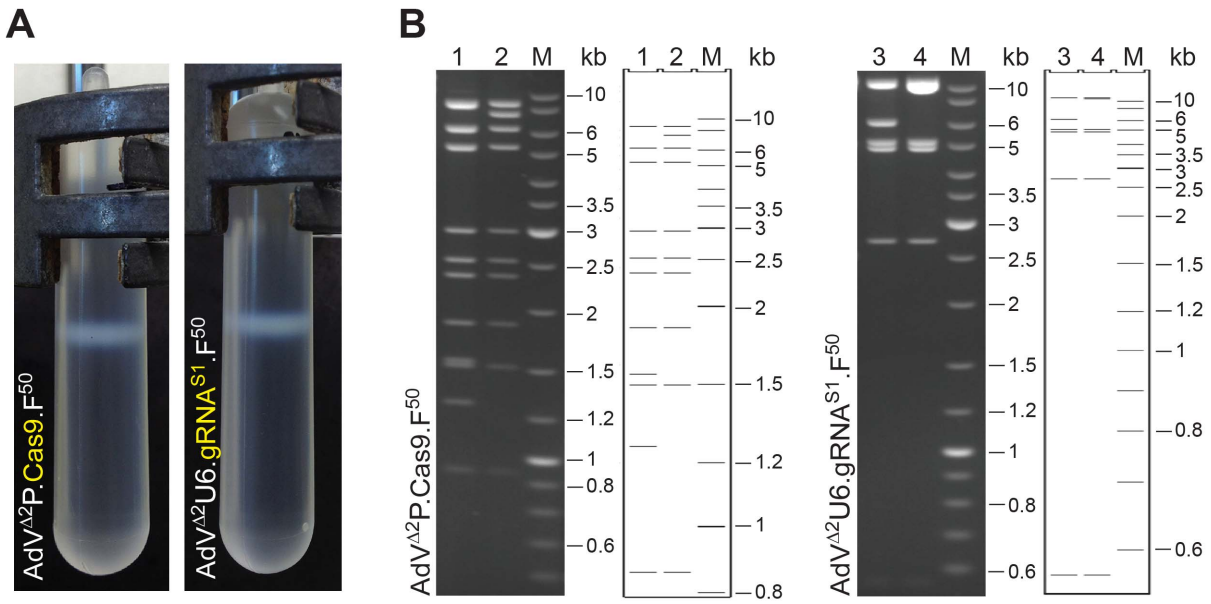

Figure 3 | Structural analysis of AdV genomes. (A) Genome-containing AdV particles after ultracentrifugation banding through continuous CsCl density gradients (B) Characterization by restriction fragment length analysis of DNA isolated from CsCl-purified AdV particles. Left panels, in-gel and *in silico* restriction patterns of AdV$^{\Delta 2}$P.Cas9.F^{50} genomes (lanes 1) and respective pAdV$^{\Delta 2}$PGK.Cas9.F^{50} parental plasmid (lanes 2) treated with BglII. Right panel, in-gel and *in silico* restriction patterns of AdV$^{\Delta 2}$U6.gRNA^{S1}.F^{50} DNA (lanes 3) and corresponding pAdV$^{\Delta 2}$U6.sgRNA^{S1}.F^{50} parental plasmid (lanes 4) digested with Bsp1407I. Lanes M, Gene Ruler DNA Ladder marker.

frequencies resulting from different combined dosages of AdV$^{\Delta 2}$P.Cas9.F^{50} and AdV$^{\Delta 2}$U6.gRNA^{GFP}.F^{50}. Direct fluorescence microscopy (Fig. 8A) as well as flow cytometry (Figs. 8B and 8C), revealed a clear dose-dependent increase in *eGFP* disruption levels varying from a minimum of 0.8% to a maximum of 65%. Controls consisting of H27 cells transduced either with AdV$^{\Delta 2}$P.Cas9.F^{50} or with AdV$^{\Delta 2}$U6.gRNA^{GFP}.F^{50}, each applied at an MOI of 100 TU/cell, did not yield frequencies of eGFP-negative cells above background levels (Fig. 8B).

Taken our data together, we conclude that AdVs encoding RGN components can be produced to high titers and achieve robust targeted mutagenesis in a diverse array of human cell types.

Discussion

One can postulate that AdV technologies, in addition to their utility in well-established biomedical research fields such as oncology and vaccinology[24–26], will start having an increasing role in experimental and applied genome engineering as well. An initial effort in this direction is provided by an AIDS therapeutic strategy based on knocking out the HIV-1 co-receptor gene *CCR5* following AdV-mediated *ZFN* transfer into CD4$^+$ T cells cultured *ex vivo*[27]. Related to this, we have recently shown that AdVs can also serve as delivery vehicles for introducing functional TALENs into human cells[18], whereas Ebina and colleagues have provided a proof-of-concept for using RGNs to disrupt HIV-1 proviral DNA[28]. In the current work, we have extended the utility of the AdV technology to genome engineering strategies based on RNA-dependent DNA nucleases derived from a type II CRISPR/Cas system.

Assuming that designer nuclease gene expression should ideally occur at high levels[29,30] and be short-term, AdVs may ultimately be preferable expression platforms when compared to other episomal viral vector systems such as silencing-prone integrase-defective lentiviral vectors (IDLVs)[30,31] and ssDNA adeno-associated viral vectors (AAVs)[32]. Moreover, the relatively large size of *Cas* ORFs may, to some extent, compromise the production of viral vectors whose optimal nucleic acid packaging capacities are significantly lower than those offered by AdV backbones and capsids. Still related to this payload capacity issue, our results further suggest that efficient chromosomal DSB formation seems to display a higher dependency on the overall RGN concentrations in target cell nuclei rather than on the use of a specific ratio between the Pol-II and Pol-III expression units. Thus, integrated vector designs in which both *Cas9* and *gRNA* expression units are co-delivered within single vector particles may turn out to be advantageous in certain experimental settings.

By carrying out transduction experiments with AdVs encoding validated gRNA^{S1}:Cas9 complexes and optimized TALEN-L^{S1}:TALEN-R^{S1} heterodimers, we found that the latter sequence-specific nuclease system yielded gene disruption levels that were similar to or higher than those achieved by the former. This outcome is different from that reported recently by Ding and colleagues[33]. Through co-transfection experiments in human pluripotent stem cell lines comparing gRNA:Cas9 sets with TALEN pairs based on specific architectures, these authors showed that, for each targeted locus, the RGNs consistently and substantially outperformed the TALENs. At this stage it is difficult to pinpoint any culprit(s) for these different outcomes since the variables are numerous and include the nature of the scaffolds for each platform, the delivery methods as well as the cell types and chromosomal target sequences tested. Nonetheless, our results do support the view that the TALEN platform is not *per se* inferior to that of RGNs in what site-specific chromosomal cleaving activity is concerned. Finally, we have shown that, at matched doses, AdV-mediated transfer of the *AAVS1*-specific RGNs led to higher gene disruption levels in myoblasts than in hMSCs. Whether these data are a consequence of different epigenetic signatures at *AAVS1* or some other cell type-specific variable(s) remains to be investigated.

In conclusion, our findings demonstrate that AdVs constitute a valuable delivery option for introducing type II CRISPR/Cas-derived RGN complexes into human cells regardless of their transformation status and open as a result the perspective for RGN deployment and optimization in human primary cells. This research might include, in addition to on-target versus off-target assessments and gene knockout approaches, the testing of genome editing strategies based on donor DNA templates and AdV delivery of RGNs into target cell nuclei.

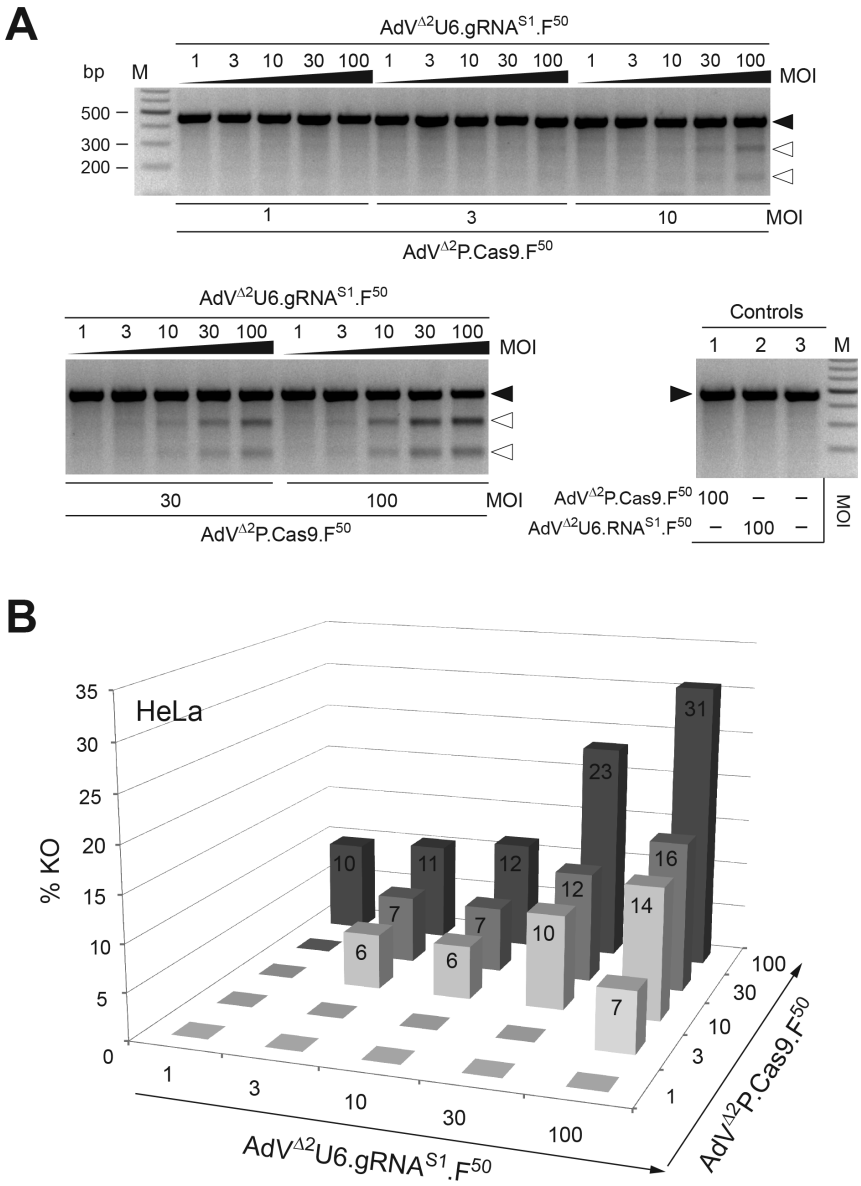

Figure 4 | Transduction experiments in HeLa cells for the functional validation of AdV$^{\Delta 2}$P.Cas9.F^{50} and AdV$^{\Delta 2}$U6.gRNA^{S1}.F^{50}. (A) Genotyping assays based on the detection of indels generated by NHEJ-mediated DSB repair at the chromosomal target site. The *AAVS1*-specific amplicons derived from genomic DNA of HeLa cells co-transduced with AdV$^{\Delta 2}$P.Cas9.F^{50} and AdV$^{\Delta 2}$U6.gRNA^{S1}.F^{50} at the indicated MOIs (in TU/cell) were denaturated and re-annealed, treated with T7EI and resolved through agarose gel electrophoresis. As negative controls, it was used genomic DNA isolated from HeLa cells exposed to 100 TU/cell of AdV$^{\Delta 2}$P.Cas9.F^{50} (lane 1), 100 TU/cell of AdV$^{\Delta 2}$U6.gRNA^{S1}.F^{50} (lane 2) or to no vector (lane 3). Solid and open arrowheads indicate the positions of undigested and T7EI-digested DNA molecules, respectively. Lane M, Gene Ruler DNA Ladder marker. (B) Target gene knockout frequencies in HeLa cells co-transduced with AdV$^{\Delta 2}$P.Cas9.F^{50} and AdV$^{\Delta 2}$U6.gRNA^{S1}.F^{50} as measured by densitometry of the DNA species depicted in Fig. 4A.

Methods

Cells. The U2OS human osteosarcoma and the HeLa cervix carcinoma cells (American Type Culture Collection) were cultured in Dulbecco's modified Eagle's medium (DMEM) containing 10% and 5% fetal bovine serum (FBS), respectively, at 37°C in a 10% CO_2 atmosphere. The *E1*- and *E2A*-complementing AdV packaging cell line PER.E2A[34], was kept in DMEM supplemented with 10% FBS, 10 mM $MgCl_2$ and 250 μg/ml of Geneticin (Invitrogen). PER.E2A cells were regularly sub-cultured at 39°C and were shifted to 34°C during AdV production for the proper folding of their *E2A*-encoded thermo-sensitive DNA-binding protein. The origin of and culture conditions for the HeLa cell-derived clone H27, constitutively expressing *eGFP*, as well as those for myoblasts and hMSCs have been detailed elsewhere[23,35,36]. PER.C6 cells[37] were cultured at 37°C in DMEM with 10% FBS and 10 mM $MgCl_2$.

Recombinant DNA. Standard recombinant DNA techniques were applied for the construction of the various AdV shuttle plasmids[38]. The TALEN-encoding plasmids pAdSh.PGK.TALEN-L^{S1} [39] and pAdSh.PGK.TALEN-R^{S1} [39] harbor the *TALEN* ORFs derived from 1383.pVAX.AAVS1.TALEN.L-94[18] and 1384.pVAX.AAVS1.TALEN.R-95[18], respectively. These constructs contain as transcription regulatory elements the human house-keeping phosphoglycerate kinase 1 gene (*PGK*) promoter and the simian virus 40 polyadenylation signal (SV40)[39]. The pAdSh.PGK.Cas9 and pSh.AAVS1.eGFP[40] constructs have these *PGK* and SV40 regulatory elements controlling the human codon-optimized ORF encoding hCas9[10] (herein referred to as Cas9) and the reporter eGFP, respectively. The *Cas9* ORF was isolated from Addgene plasmid 41815. The expression units gRNA_AAVS1-T2[10] and gRNA_GFP-T2[10] based on the *U6* RNA Pol III promoter (herein dubbed gRNA^{S1} and gRNA^{GFP}, respectively) were retrieved from Addgene plasmids 41818 and 41820 and were inserted into the MCS of pAdSh.MCS.SV40, resulting in constructs pAdSh.U6.gRNA^{S1} and pAdSh.U6.gRNA^{GFP}, respectively.

The *E1*- and *E2A*-deleted (i.e. second-generation) fiber-modified AdV molecular clones pAdV$^{\Delta 2}$P.TALEN-L^{S1}.F^{50}, pAdV$^{\Delta 2}$P.TALEN-R^{S1}.F^{50}, pAdV$^{\Delta 2}$P.Cas9.F^{50}, pAdV$^{\Delta 2}$U6.gRNA^{S1}.F^{50}, pAdV$^{\Delta 2}$U6.gRNA^{GFP}.F^{50} and pAdV$^{\Delta 2}$P.eGFP.F^{50} were assembled via homologous recombination after transformation of BJ5183$^{pAdEasy\text{-}2.50}$ *E.*

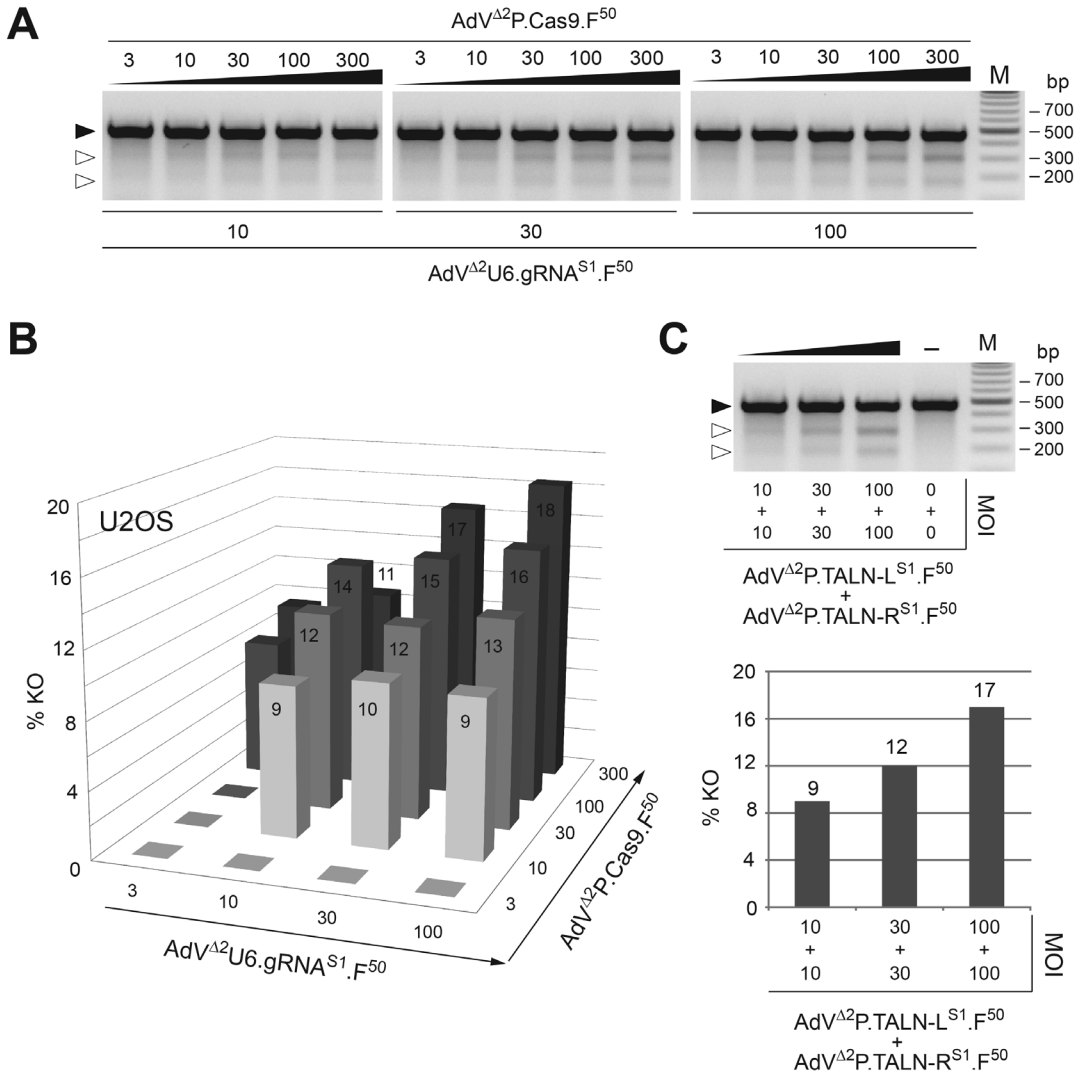

Figure 5 | Analyses of site-specific DSB formation in U2OS cells following AdV-mediated delivery of transgenes encoding RGN and TALEN complexes. (A) Targeted mutagenesis experiments with AdV$^{\Delta 2}$P.Cas9.F^{50} and AdV$^{\Delta 2}$U6.gRNA^{S1}.F^{50}. Agarose gel electrophoresis of *AAVS1*-specific PCR products amplified from chromosomal DNA of U2OS cells co-transduced with the indicated MOIs of AdV$^{\Delta 2}$P.Cas9.F^{50} and AdV$^{\Delta 2}$U6.gRNA^{S1}.F^{50} (in TU/cell). Prior to loading the PCR products were denaturated, re-annealed and treated with the mismatch-sensitive enzyme T7EI. Solid and open arrowheads point to the positions of undigested and T7EI-digested DNA molecules, respectively. Lane M, Gene Ruler DNA Ladder marker. (B) Target gene knockout frequencies in U2OS cells co-transduced with AdV$^{\Delta 2}$P.Cas9.F^{50} and AdV$^{\Delta 2}$U6.gRNA^{S1}.F^{50} as measured by densitometry of the DNA species shown in Fig. 5A. (C) Targeted mutagenesis experiments with AdV$^{\Delta 2}$P.TALEN-L^{S1}.F^{50} and AdV$^{\Delta 2}$P.TALEN-R^{S1}.F^{50}. Upper panel, T7EI-based assays on *AAVS1*-specific amplicons corresponding to genomic DNA of mock-transduced U2OS cells (−) or of U2OS cells co-transduced with the specified MOIs of AdV$^{\Delta 2}$P.TALEN-L^{S1}.F^{50} and AdV$^{\Delta 2}$P.TALEN-R^{S1}.F^{50} (in TU/cell). Solid and open arrowheads indicate the positions of undigested and T7EI-digested DNA molecules, respectively. Lanes M, Gene Ruler DNA Ladder marker. Lower panel, target gene knockout frequencies in U2OS cells co-transduced with AdV$^{\Delta 2}$P.TALEN-L^{S1}.F^{50} and AdV$^{\Delta 2}$P.TALEN-R^{S1}.F^{50} as determined by densitometry of the DNA fragments presented in the upper panel.

coli cells[41] with MssI-treated AdV shuttle plasmids pAdSh.PGK.TALEN-L^{S1}, pAdSh.PGK.TALEN-R^{S1}, pAdSh.PGK.Cas9, pAdSh.U6.gRNA^{S1}, pAdSh.U6.gRNA^{GFP} and pSh.AAVS1.eGFP[40], respectively.

Validation of Cas9- and gRNA^{S1}-encoding AdV shuttle plasmids. PER.C6 cells were plated at a density of 1.5 × 10^6 cells per well of 6-well plates (Greiner Bio-One). The next day, a total amount of 6 μg of DNA corresponding to 1 : 1 mixtures of hCas9 (Addgene plasmid 41815) and gRNA_AAVS1-T2 (Addgene plasmid 41818), pAdSh.PGK.Cas9 and pAdSh.U6.gRNA^{S1}, hCas9 and gRNA_Cloning Vector (Addgene plasmid 41824) or hCas9_D10A (Addgene plasmid 41816) and gRNA_AAVS1-T2, were transfected by deploying a 1 mg/ml polyethyleneimine (PEI) solution (Polysciences) essentially as described elsewhere[41] except for the use of 6 μg of DNA and 19.7 μl of PEI instead of 6.25 μg of DNA and 18.8 μl of PEI. At 3 days post-transfection genomic DNA from mock-transfected cells and from co-transfected cells, was isolated according to a previously described method[42]. Targeted gene disruption was assessed by using the T7EI-based assay as described below.

Viral vector production, purification and titration. The production of viral vectors AdV$^{\Delta 2}$P.TALEN-L^{S1}.F^{50}, AdV$^{\Delta 2}$P.TALEN-R^{S1}.F^{50}, AdV$^{\Delta 2}$P.Cas9.F^{50}, AdV$^{\Delta 2}$U6.gRNA^{S1}.F^{50}, AdV$^{\Delta 2}$U6.gRNA^{GFP}.F^{50} and AdV$^{\Delta 2}$P.eGFP.F^{50}, was carried out essentially as described elsewhere[41]. In brief, the rescue of AdV particles was initiated by transfecting 1.25 × 10^6 PER.E2A cells seeded in medium without Geneticin in wells of 6-well plates (Greiner Bio-One). The next day, the cells were transfected by using 18.8 μl of a 1 mg/ml PEI solution and 6.25 μg of PacI-linearized plasmids pAdV$^{\Delta 2}$P.TALEN-L^{S1}.F^{50}, pAdV$^{\Delta 2}$P.TALEN-R^{S1}.F^{50}, pAdV$^{\Delta 2}$P.Cas9.F^{50}, pAdV$^{\Delta 2}$U6.gRNA^{S1}.F^{50}, pAdV$^{\Delta 2}$U6.gRNA^{GFP}.F^{50} and pAdV$^{\Delta 2}$P.eGFP.F^{50}. Following an overnight incubation period at 39°C, the transfection media was replaced and the cells were transferred to the permissive temperature of 34°C. After the emergence of complete cytopathic effect (CPE), the producer cells were harvested and subjected to three cycles of freezing and thawing in liquid N_2 and in a 37°C water bath, respectively. Rescued AdVs present in clarified producer cell supernatants, were subsequently amplified through propagation on newly seeded PER.E2A cells. Large-scale AdV stocks were prepared by infecting producer cells at 70-80% confluence in 16 175-cm^2

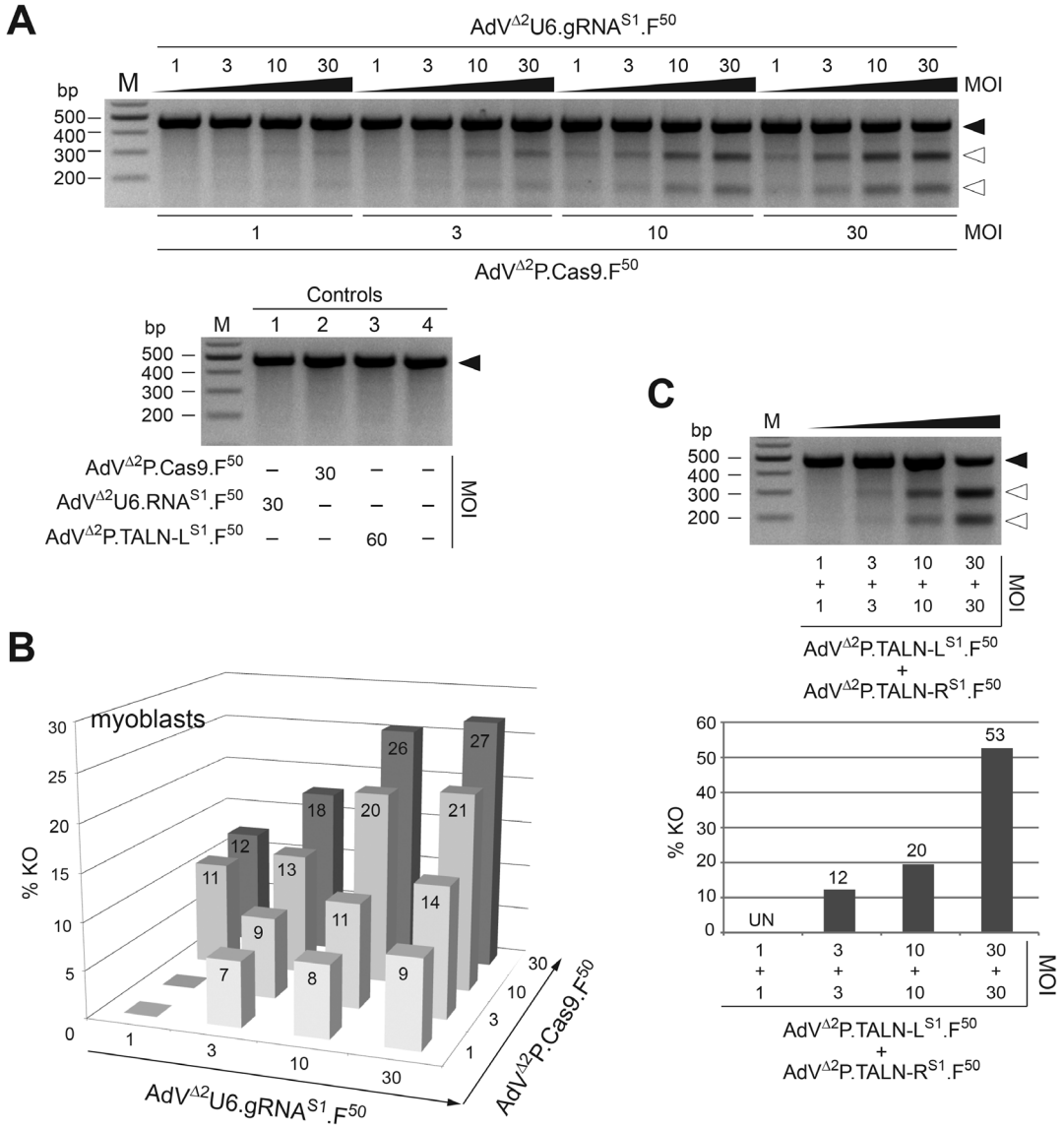

Figure 6 | Analyses of targeted mutagenesis in human myoblasts following AdV-mediated transfer of DNA coding for RGN and TALEN complexes. (A) Targeted mutagenesis experiments with AdV$^{\Delta 2}$P.Cas9.F^{50} and AdV$^{\Delta 2}$U6.gRNA^{S1}.F^{50}. Upper panel, *AAVS1*-specific PCR products corresponding to genomic DNA of myoblasts co-transduced with the indicated MOIs of AdV$^{\Delta 2}$P.Cas9.F^{50} and AdV$^{\Delta 2}$U6.gRNA^{S1}.F^{50} (in TU/cell) subjected to T7EI-based assays. Lower panel, negative controls corresponding to human myoblasts that were singly transduced with AdV$^{\Delta 2}$P.Cas9.F^{50} (lane 1), AdV$^{\Delta 2}$U6.gRNA^{S1}.F^{50} (lane 2) or AdV$^{\Delta 2}$P.TALEN-L^{S1}.F^{50} (lane 3) or that were mock-transduced (lane 4). (B) Target gene knockout frequencies in human myoblasts co-transduced with AdV$^{\Delta 2}$P.Cas9.F^{50} and AdV$^{\Delta 2}$U6.gRNA^{S1}.F^{50} as measured by densitometry of the DNA species depicted in Fig. 6A. (C) Targeted mutagenesis experiments with AdV$^{\Delta 2}$P.TALEN-L^{S1}.F^{50} and AdV$^{\Delta 2}$P.TALEN-R^{S1}.F^{50}. Upper panel, T7EI-based assays on *AAVS1*-specific amplicons obtained from genomic DNA of myoblasts co-transduced with the indicated MOIs of AdV$^{\Delta 2}$P.TALEN-L^{S1}.F^{50} and AdV$^{\Delta 2}$P.TALEN-R^{S1}.F^{50} (in TU/cell). Solid and open arrowheads indicate the positions of undigested and T7EI-digested DNA molecules, respectively. Lanes M, Gene Ruler DNA Ladder marker. Lower panel, target gene disruption frequencies in myoblasts co-transduced with AdV$^{\Delta 2}$P.TALEN-L^{S1}.F^{50} and AdV$^{\Delta 2}$P.TALEN-R^{S1}.F^{50} as determined by densitometry of the DNA fragments shown in the upper panel.

cell cultures flasks (Greiner Bio-One). The details on the isopycnic CsCl density-gradient ultracentrifugation and ultrafiltration used to purify and de-salt AdV preparations, respectively, have been described before[41]. The titers of purified AdV stocks were determined by $TCID_{50}$ assays as follows. One hundred microliters of a PER.E2A cell suspension containing 5.0×10^4 cells/ml in DMEM containing 2% FBS and 10 mM $MgCl_2$, were dispensed in wells of 96-well plates (Greiner Bio-One). After an overnight incubation period at 39°C in a 10% CO_2 atmosphere, the cells were exposed in octuplicate to 100 µl of 10-fold dilutions (range: 10^{-5} through 10^{-12}) of the various viral vector preparations. Next, the cells were incubated for 2.5 weeks at 34°C in a 10% CO_2 atmosphere having 100 µl of DMEM containing 2% FBS and 10 mM $MgCl_2$ being added at 1 week post-infection. After this incubation period, wells with cultures containing viral plaques or at full CPE were scored to calculate the titers in terms of transducing units per ml (TU/ml) as specified elsewhere[41].

Isolation of viral vector DNA for structural analysis. The isolation of AdV genomes from purified particles was carried out as specified elsewhere[41]. The *in silico* restriction patterns were made with the aid of Gene Construction kit (version 2.5) software (Textco BioSoftware, Inc.).

Transduction experiments. Myoblasts, hMSCs and U2OS cells were seeded in their respective media at a density of 1×10^5 cells per well of 24-well plates (Greiner Bio-One), whereas HeLa cells were plated in the same vessel format at a density of 5×10^4 cells. Approximately 24 hours after seeding, the cells were exposed in 500-µl volumes to the two different AdV pair combinations (i.e. AdV$^{\Delta 2}$P.TALEN-L^{S1}.F^{50}/AdV$^{\Delta 2}$P.TALEN-R^{S1}.F^{50} or AdV$^{\Delta 2}$P.Cas9.F^{50}/AdV$^{\Delta 2}$U6.gRNA^{S1}.F^{50}) at the indicated multiplicities of infection (MOI). Mock-transduced cells or, whenever indicated, cells transduced exclusively with one element of each vector pair, served as negative

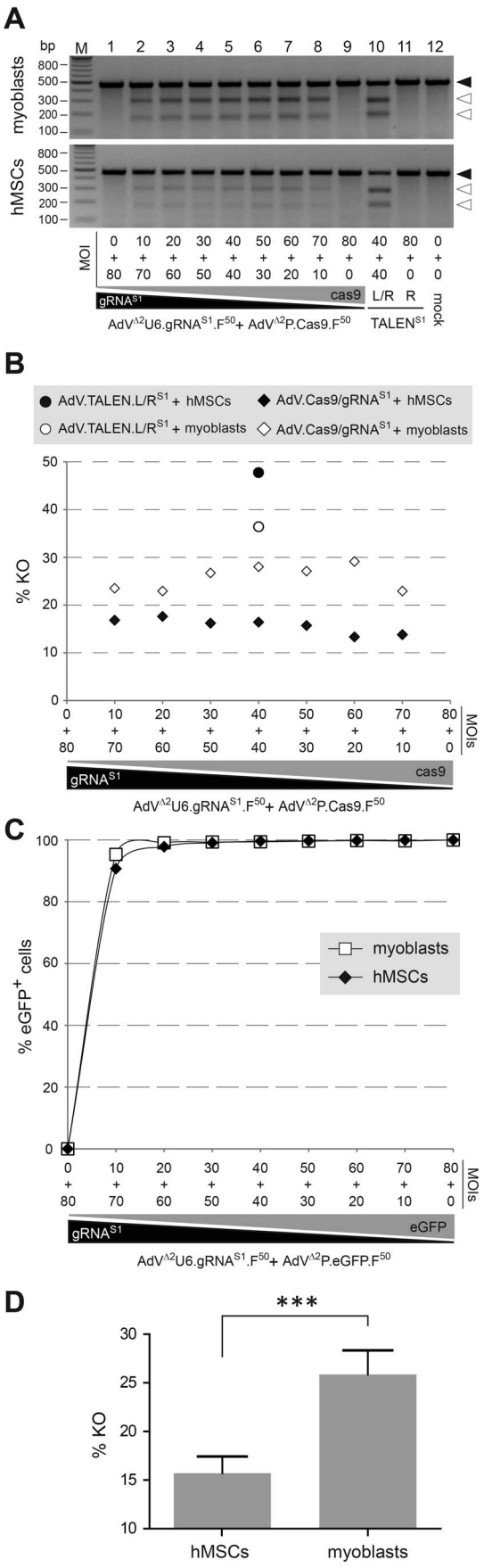

Figure 7 | Analyses of target gene knockout frequencies following AdV-mediated introduction of gRNA^{S1}:Cas9 and TALEN-L^{S1}:TALEN-R^{S1} complexes into hMSCs versus human myoblasts. (A) Target site genotyping assays. Upper and lower panels, agarose gel electrophoresis of *AAVS1*-specific PCR products amplified from chromosomal DNA of myoblasts and hMSCs, respectively, co-transduced with the indicated MOIs of AdV$^{\Delta 2}$P.Cas9.F^{50} and AdV$^{\Delta 2}$U6.gRNA^{S1}.F^{50} (in TU/cell). Before loading the amplicons were denaturated, re-annealed and treated with the mismatch-sensitive enzyme T7EI. The cells were co-transduced at a combined MOI of 80 TU/cell with different ratios of AdV$^{\Delta 2}$P.Cas9.F^{50} and AdV$^{\Delta 2}$U6.gRNA^{S1}.F^{50} or with 1 : 1 mixtures of AdV$^{\Delta 2}$P.TALEN-L^{S1}.F^{50} and AdV$^{\Delta 2}$P.TALEN-R^{S1}.F^{50}. Mock-transduced cells or cells exposed to 80 TU/cell of AdV$^{\Delta 2}$P.Cas9.F^{50}, AdV$^{\Delta 2}$U6.gRNA^{S1}.F^{50} or AdV$^{\Delta 2}$P.TALEN-L^{S1}.F^{50} served as negative controls. Solid and open arrowheads indicate the positions of undigested and T7EI-digested amplicons, respectively. Lanes M, Gene Ruler DNA Ladder marker. (B) Target gene knockout activities in hMSCs and myoblasts transduced with AdVs. Target gene disruption frequencies in cells co-transduced with AdV pairs AdV$^{\Delta 2}$P.Cas9.F^{50}/AdV$^{\Delta 2}$U6.gRNA^{S1}.F^{50} and AdV$^{\Delta 2}$P.TALEN-L^{S1}.F^{50}/AdV$^{\Delta 2}$P.TALEN-R^{S1}.F^{50} as determined by densitometry of DNA fragments depicted in Fig. 7A. (C) Gene delivery activities in hMSCs and myoblasts transduced with AdVs. Percentages of transduced cells incubated with different mixtures of reporter vector AdV$^{\Delta 2}$P.eGFP.F^{50} and AdV$^{\Delta 2}$U6.gRNA^{S1}.F^{50}, applied at a combined MOI of 80 TU/cell. Cells exposed only to AdV$^{\Delta 2}$U6.gRNA^{S1}.F^{50} at an MOI of 80 TU/cell served as negative controls. The frequency of eGFP-positive cells was determined by flow cytometry at three days post-transduction. (D) Cumulative data corresponding to the gene knockout frequencies in hMSCs versus human myoblasts following AdV-mediated delivery of gRNA^{S1}:Cas9 complexes into these cells. Plotted data show the mean ± standard deviation (n = 7).

controls. Three days post-infection, total cellular DNA was isolated by using the DNeasy Blood & Tissue kit (Qiagen) following the manufacturer's recommendations.

Transduction experiments on indicator H27 cells. One day before transduction, 1.0 × 10^5 H27 cells were seeded in wells of 24-well plates. After the removal of the culture medium, the H27 cell monolayers were incubated in 500-µl volumes consisting of various total and relative amounts of AdV$^{\Delta 2}$P.Cas9.F^{50} and AdV$^{\Delta 2}$U6.gRNA^{GFP}.F^{50}. Mock-transduced H27 cells and H27 cells exposed exclusively to AdV$^{\Delta 2}$P.Cas9.F^{50} or to AdV$^{\Delta 2}$U6.gRNA^{GFP}.F^{50} each applied at an MOI of 100 TU/cell, provided for negative controls. Subsequently, after extensive sub-culturing to remove reporter protein from cells with disrupted *eGFP* ORFs, the presence of eGFP-negative cells was assessed by direct fluorescence microscopy and flow cytometry at 15 days post-transduction.

Direct fluorescence microscopy. Targeted *eGFP* knockout in H27 cell cultures was monitored by direct fluorescence microscopy. The H27 cell nuclei were stained by adding Hoechst 33342 (Molecular Probes) at 10 µg/ml for 10 min. Next, the cell cultures were washed twice with PBS, after which culture medium was added. The eGFP- and Hoechst 33342-specific signals were detected by using an Olympus IX51 inverse fluorescence microscope (Olympus). Micrographs were captured and archived by deploying a XC30 Peltier CCD camera and the CellF software (both from Olympus).

Flow cytometry. The frequencies of eGFP-positive cells in cultures transduced with AdV$^{\Delta 2}$P.eGFP.F^{50} and of eGFP-negative cells in H27 cell cultures were determined by using a BD LSR II flow cytometer (BD Biosciences). Data were analyzed with the aid of FlowJo 7.2.2 software (Tree Star). Mock-transduced H27 cells served to establish the cut-off between eGFP-positive and eGFP-negative cell populations. Samples of at least 10,000 viable single cells were analyzed per experimental condition.

T7 endonuclease I-based genotyping assays. Target gene disruption levels were assessed by using mismatch-sensitive T7EI. To this end, genomic DNA samples from target cells were subjected to PCR for the amplification of a 469-bp DNA segment encompassing the target sites for the gRNA^{S1}:Cas9 and TALEN-L^{S1}:TALEN-R^{S1} complexes. The primers, PCR reagents and cycling conditions used have been described in detail before[18]. Next, the resulting amplicons were denaturated and reannealed in a thermocycler by applying the program specified in Supplementary Table S1. One fifth of each PCR mixture was incubated in 15-µl reactions with 1 × NEBuffer 2 and 5 U of T7EI (both from New England Biolabs). Control reactions lacked T7EI. After 15 minutes at 37°C, the samples were subjected to electrophoresis through 2% (w/v) agarose in 1 × Tris-Acetate-EDTA buffer. Finally, ethidium bromide-stained DNA species were measured in a Molecular Imager Gel-Doc™ XR+ with the aid of Bio-Rad Image Lab 4.1 software (both from Bio-Rad).

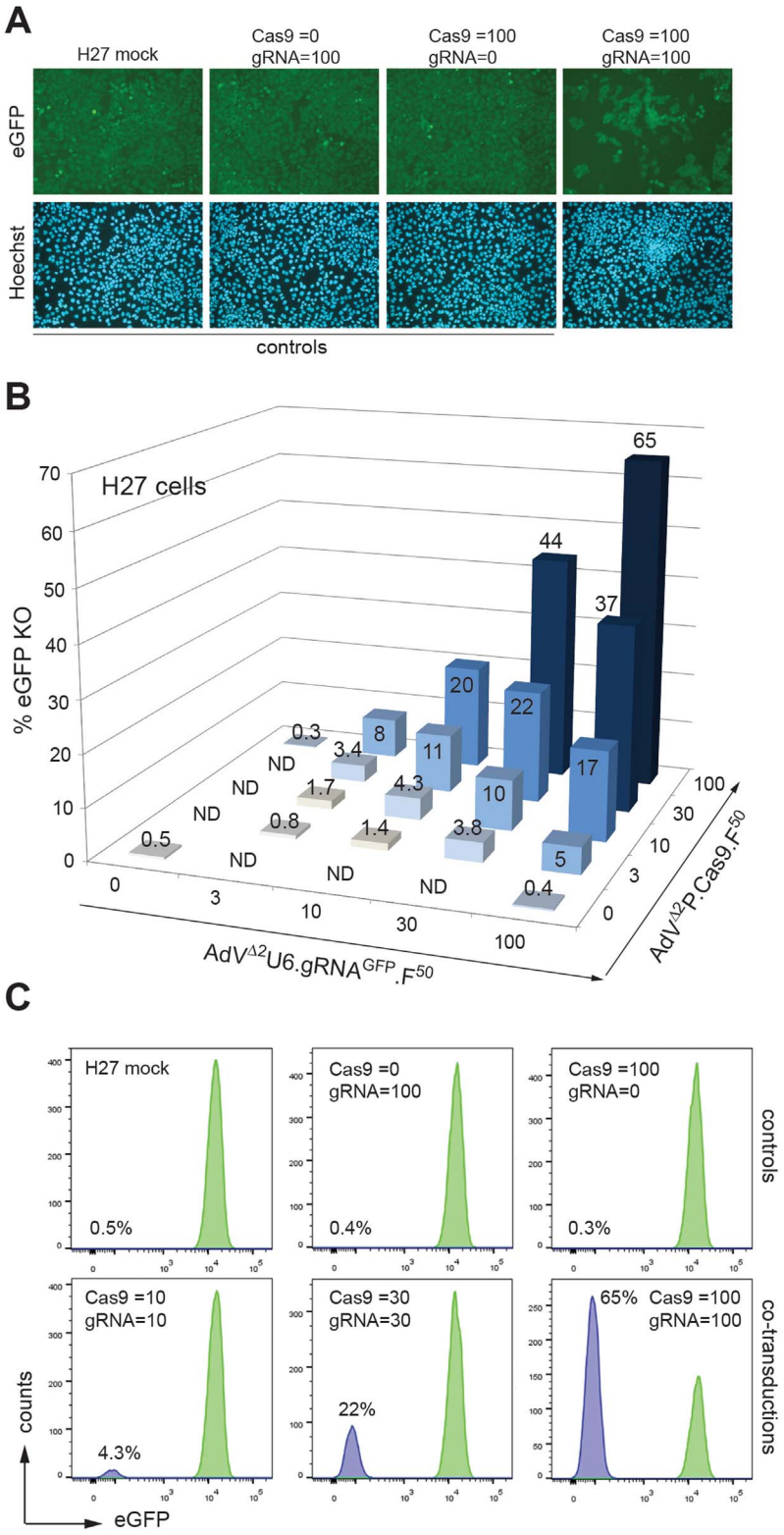

Figure 8 | Analyses of target gene editing frequencies in human H27 cells transduced with AdVs encoding *eGFP*-directed RGN complexes. (A) Fluorescence microscopy on cultures of *eGFP*-expressing H27 cells co-transduced with a 1 : 1 mixture of AdV$^{\Delta 2}$P.Cas9.F^{50} and AdV$^{\Delta 2}$U6.gRNA^{GFP}.F^{50} applied at total MOI of 200 TU/cell (Cas9 = 100; gRNA = 100). Negative controls consisted of mock-transduced H27 cells and of H27 cells transduced with AdV$^{\Delta 2}$U6.gRNA^{GFP}.F^{50} alone at an MOI of 100 TU/cell (Cas9 = 0; gRNA = 100) or with AdV$^{\Delta 2}$P.Cas9.F^{50} alone at an MOI of 100 TU/cell (Cas9 = 100; gRNA = 0). Cell nuclei and *eGFP*-expressing cells in each field were identified via Hoechst 33342- and *eGFP*-directed fluorescence microscopy, respectively. Note the presence of eGFP-negative cells in cultures transduced with both vector types. (B) Flow cytometry-based quantification of target gene knockout levels in H27 cell cultures transduced with AdV$^{\Delta 2}$P.Cas9.F^{50} and AdV$^{\Delta 2}$U6.gRNA^{GFP}.F^{50} at the indicated MOIs (in TU/cell). ND, not done. (C) Representative flow cytometry histograms corresponding to data points presented in Fig. 8B. The analyses of target gene knockout by fluorescence microscopy and flow cytometry were both performed at 15 days post-transduction.

1. Gaj, T., Gersbach, C. A. & Barbas, C. F. 3rd. ZFN, TALEN, and CRISPR/Cas-based methods for genome engineering. *Trends Biotechnol.* **31**, 397–405 (2013).
2. Segal, D. J. & Meckler, J. F. Genome engineering at the dawn of the golden age. *Annu. Rev. Genomics Hum. Genet.* **14**, 135–158 (2013).
3. Biasco, L., Baricordi, C. & Aiuti, A. Retroviral integrations in gene therapy trials. *Mol. Ther.* **20**, 709–716 (2012).
4. Bhaya, D., Davison, M. & Barrangou, R. CRISPR-Cas systems in bacteria and archaea: versatile small RNAs for adaptive defense and regulation. *Annu. Rev. Genet.* **45**, 273–297 (2011).
5. Wiedenheft, B., Sternberg, S. H. & Doudna, J. A. RNA-guided genetic silencing systems in bacteria and archaea. *Nature* **482**, 331–338 (2012).
6. Gasiunas, G., Barrangou, R., Horvath, P. & Siksnys, V. Cas9-crRNA ribonucleoprotein complex mediates specific DNA cleavage for adaptive immunity in bacteria. *Proc. Natl. Acad. Sci. USA* **109**, E2579–E2586 (2012).
7. Jinek, M. *et al.* A programmable dual-RNA-guided DNA endonuclease in adaptive bacterial immunity. *Science* **337**, 816–821 (2012).
8. Cong, L. *et al.* Multiplex genome engineering using CRISPR/Cas systems. *Science* **339**, 819–823 (2013).
9. Jinek, M. *et al.* RNA-programmed genome editing in human cells. *Elife* **2**, e00471 (2013).
10. Mali, P. *et al.* RNA-guided human genome engineering via Cas9. *Science* **339**, 823–826 (2013).
11. Gasiunas, G. & Siksnys, V. RNA-dependent DNA endonuclease Cas9 of the CRISPR system: Holy Grail of genome editing? *Trends Microbiol.* **21**, 562–567 (2013).
12. Cradick, T. J., Fine, E. J., Antico, C. J. & Bao, G. CRISPR/Cas9 systems targeting β-globin and CCR5 genes have substantial off-target activity. *Nucleic Acids Res.* **41**, 9584–9592 (2013).
13. Fu, Y. *et al.* High-frequency off-target mutagenesis induced by CRISPR-Cas nucleases in human cells. *Nat. Biotechnol.* **31**, 822–826 (2013).
14. Hsu, P. D. *et al.* DNA targeting specificity of RNA-guided Cas9 nucleases. *Nat. Biotechnol.* **31**, 827–832 (2013).
15. Mali, P. *et al.* CAS9 transcriptional activators for target specificity screening and paired nickases for cooperative genome engineering. *Nat. Biotechnol.* **31**, 833–838 (2013).
16. Pattanayak, V. *et al.* High-throughput profiling of off-target DNA cleavage reveals RNA-programmed Cas9 nuclease specificity. *Nat Biotechnol.* **31**, 839–843 (2013).
17. Gonçalves, M. A. F. V. & de Vries, A. A. F. Adenovirus: from foe to friend. *Rev Med. Virol.* **16**, 167–186 (2006).
18. Holkers, M. *et al.* Differential integrity of TALE nuclease genes following adenoviral and lentiviral vector gene transfer into human cells. *Nucleic Acids Res.* **41**, e63 (2013).
19. Shayakhmetov, D. M., Papayannopoulou, T., Stamatoyannopoulos, G. & Lieber, A. Efficient gene transfer into human CD34(+) cells by a retargeted adenovirus vector. *J. Virol.* **74**, 2567–2583 (2000).
20. Knaän-Shanzer, S. *et al.* Highly efficient targeted transduction of undifferentiated human hematopoietic cells by adenoviral vectors displaying fiber knobs of subgroup B. *Hum. Gene Ther.* 12, 1989–2005 (2001). Erratum in: *Hum. Gene Ther.* **14**, 1214 (2003).
21. Knaän-Shanzer, S. *et al.* Endowing human adenovirus serotype 5 vectors with fiber domains of species B greatly enhances gene transfer into human mesenchymal stem cells. *Stem Cells* **23**, 1598–1607 (2005).
22. Gonçalves, M. A. F. V. *et al.* Transduction of myogenic cells by retargeted dual high-capacity hybrid viral vectors: robust dystrophin synthesis in duchenne muscular dystrophy muscle cells. *Mol. Ther.* **13**, 976–986 (2006).
23. Gonçalves, M. A. F. V., van der Velde, I., Knaän-Shanzer, S., Valerio, D. & de Vries, A. A. F. Stable transduction of large DNA by high-capacity adeno-associated virus/adenovirus hybrid vectors. *Virology* **321**, 287–296 (2004).
24. Barouch, D. H. & Nabel, G. J. Adenovirus vector-based vaccines for human immunodeficiency virus type 1. *Hum. Gene Ther.* **16**, 149–156 (2005).
25. Post, D. E., Khuri, F. R., Simons, J. W. & van Meir, E. G. Replicative oncolytic adenoviruses in multimodal cancer regimens. *Hum. Gene Ther.* **14**, 933–946 (2003).
26. Aurisicchio, L. & Ciliberto, G. Genetic cancer vaccines: current status and perspectives. *Expert. Opin. Biol. Ther.* **12**, 1043–1058 (2012).
27. Perez, E. E. *et al.* Establishment of HIV-1 resistance in CD4+ T cells by genome editing using zinc-finger nucleases. *Nat. Biotechnol.* **26**, 808–816 (2008).
28. Ebina, H., Misawa, N., Kanemura, Y. & Koyanagi, Y. Harnessing the CRISPR/Cas9 system to disrupt latent HIV-1 provirus. *Sci. Rep.* **3**, 2510 (2013).
29. Kim, H. *et al.* Surrogate reporters for enrichment of cells with nuclease-induced mutations. *Nat. Methods* **8**, 941–943 (2011).
30. Pelascini, L. P. *et al.* Histone deacetylase inhibition rescues gene knockout levels achieved with integrase-defective lentiviral vectors encoding zinc-finger nucleases. *Hum. Gene Ther. Methods* **24**, 399–411 (2013).
31. Pelascini, L. P., Janssen, J. M. & Gonçalves, M. A. F. V. Histone deacetylase inhibition activates transgene expression from integration-defective lentiviral vectors in dividing and non-dividing cells. *Hum. Gene Ther.* **24**, 78–96 (2013).
32. Ferrari, F. K., Samulski, T., Shenk, T. & Samulski, R. J. Second-strand synthesis is a rate-limiting step for efficient transduction by recombinant adeno-associated virus vectors. *J. Virol.* **70**, 3227–3234 (1996).
33. Ding, Q. *et al.* Enhanced efficiency of human pluripotent stem cell genome editing through replacing TALENs with CRISPRs. *Cell Stem Cell* **12**, 393–394 (2013).
34. Havenga, M. J. *et al.* Serum-free transient protein production system based on adenoviral vector and PER.C6 technology: high yield and preserved bioactivity. *Biotechnol. Bioeng.* **100**, 273–283 (2008).
35. Cudré-Mauroux, C. *et al.* Lentivector-mediated transfer of Bmi-1 and telomerase in muscle satellite cells yields a duchenne myoblast cell line with long-term genotypic and phenotypic stability. *Hum. Gene Ther.* **14**, 1525–1533 (2003).
36. Gonçalves, M. A. F. V. *et al.* Transcription factor rational design improves directed differentiation of human mesenchymal stem cells into skeletal myocytes. *Mol. Ther.* **19**, 1331–1341 (2011).
37. Fallaux, F. J. *et al.* New helper cells and matched early region 1-deleted adenovirus vectors prevent generation of replication-competent adenoviruses. *Hum. Gene Ther.* **9**, 1909–1917 (1998).
38. Sambrook, J. F. & Russell, D. W. *Molecular Cloning: A Laboratory Manual, 3rd Ed.* Sambrook, J. F. & Russell, D. W. (eds.) (Cold Spring Harbor Laboratory Press, Cold Spring Harbor, NY, 2001).
39. Holkers, M., Cathomen, T. & Gonçalves, M. A. F. V. Construction and characterization of adenoviral vectors for the delivery of TALENs into human cells. *Methods* S1046–2023 (2014). Epub ahead of print. doi:10.1016/j.ymeth.2014.02.017.
40. Coluccio, A. *et al.* Targeted gene addition in human epithelial stem cells by zinc-finger nuclease-mediated homologous recombination. *Mol. Ther.* **21**, 1695–1704 (2013).
41. Janssen, J. M., Liu, J., Skokan, J., Gonçalves, M. A. F. V. & de Vries, A. A. F. Development of an AdEasy-based system to produce first- and second-generation adenoviral vectors with tropism for CAR- or CD46-positive cells. *J. Gene Med.* **15**, 1–11 (2013).
42. Laird, P. W. *et al.* Simplified mammalian DNA isolation procedure. *Nucleic Acids Res.* **19**, 4293 (1991).

Acknowledgments

This work was supported by the AFMTéléthon [grant number 16621] and the Prinses Beatrix Spierfonds [grant number W.OR11-18]. Xiaoyu Chen is the recipient of a Ph.D. research grant from the China Scholarship Council-Leiden University Joint Scholarship Programme. The authors would like to thank Sara F. Henriques (EU ERASMUS Programme grantee from the Faculdade de Ciências da Universidade de Lisboa [PLISBOA 02]) for constructing the Cas9-encoding AdV shuttle plasmid and Rob Hoeben (Department of Molecular Cell Biology, Leiden University Medical Center, The Netherlands) for critically reading the manuscript. The authors are also thankful to Alessandra Recchia (University of Modena and Reggio Emilia, Italy) for providing pSh.AAVS1.eGFP and to Toni Cathomen (Institute for Cell and Gene Therapy and Center for Chronic Immunodeficiency, University Medical Center Freiburg, Germany) for making available 1383.pVAX.AAVS1.TALEN.L-94 and 1384.pVAX.AAVS1.TALEN.R-95.

Author contributions

I.M. and M.H. contributed equally to this work. I.M. and M.H. performed the experiments. J.L., J.M.J. and X.C. produced and characterized reagents. I.M., M.H., J.M.J. and M.A.F.V.G. designed the experiments and analyzed the data. M.A.F.V.G. conceived and initiated the research. M.A.F.V.G. wrote the manuscript with the help from all authors.

Additional information

Supplementary information accompanies this paper at http://www.nature.com/scientificreports

Competing financial interests: The authors declare no competing financial interests.

How to cite this article: Maggio, I. *et al.* Adenoviral vector delivery of RNA-guided CRISPR/Cas9 nuclease complexes induces targeted mutagenesis in a diverse array of human cells. *Sci. Rep.* **4**, 5105; DOI:10.1038/srep05105 (2014).